ELSEVIER

Journal of Photochemistry and Photobiology A: Chemistry 141 (2001) 127–132

Journal of Photochemistry and Photobiology A:Chemistry

www.elsevier.nl/locate/jphotochem

Multiple emission of *N*-(1-naphthyl)-pyridinium

V.A. Kharlanov*, W. Rettig

Institute of Physical and Theoretical Chemistry, Humboldt University of Berlin, Bunsenstr. 1, 10117 Berlin, Germany

Received 5 January 2001; accepted 15 February 2001

Abstract

The trimethyl derivative of *N*-(1-naphthyl)-pyridinium shows temperature dependent multiple fluorescence. Quantum chemical calculations indicate that several minima on the S_1-hypersurface are responsible for this behaviour. Locally excited, resonance-type charge shift and biradicaloid charge shift states could be characterised.

Keywords: Multiple fluorescence; Electron transfer; Charge transfer; Biradicaloid structure; Pyridinium cation

1. Introduction

Our investigations [1–3] of *N*-(1-anthryl)-pyridinium **ANTPy**$^+$ (Scheme 1) have shown that this cation exhibits a weak fluorescence ($\lambda_f = 526$ nm, $\Phi_f = 0.033$, $\tau_f = 2.6$ ns, EtOH, 295 K) with a red-shifted structureless band at room temperature but with a strong short-wavelength emission in rigid matrix (anthracene-type fluorescence, $\lambda_f = 397$ nm, $\tau_f = 13.8$ ns, EtOH, 77 K) and dual emission at intermediate temperatures.

The goal of our present investigations is the study of the photophysics of an electronically closely related cation, the naphtyl derivative *N*-(1-naphthyl)-pyridinium **TMNTPy**$^+$ (Scheme 1) by steady and time resolved spectroscopy and by semiempirical and ab initio calculations.

2. Experiment and calculation

2.1. Materials

TMNTPy$^+$ was prepared in the form of the perchlorate salt (anion ClO_4^-) by known methods [4] and purified by recrystallisation. The product was checked for purity by fluorescence after each recrystallisation step as in a previous paper [3]. The solvent (ethanol) used was of spectroscopic grade quality (Merck Uvasol).

2.2. Apparatus and methods

Absorption spectra were recorded with an ATI Unicam UV2 spectrophotometer. Corrected fluorescence emission and fluorescence excitation spectra of solutions with an absorbance $A = 0.02$–0.06 were measured with a SLM AMINCO AB2 spectrofluorimeter.

Fluorescence quantum yields (±10%) were determined using naphthalene as standard ($\Phi_f = 0.23$, cyclohexane, 295 K [5]. Refractive index corrections were made [6] to adjust for the different solvents used. The quantum yield changes with temperature variation were corrected both with respect to the refractive index [7] and density [8] changes of the solvent.

The fluorescence lifetime measurements were performed with a single-photon counting equipment using synchrotron radiation from the Berlin storage ring BESSY in the single bunch mode as the excitation source, as described elsewhere [9]. The excitation wavelength ($\Delta\lambda = 20$ nm) was chosen at the maximum of the long wavelength absorption band (270 nm, $A = 0.1$–0.4). Decay times were fitted using the iterative reconvolution procedure which allowed a time resolution down to 0.1 ns and a precision of better than 0.1 ns. Satisfactory fits ($\chi^2 < 1.2$) were obtained in all cases with one, two or three exponential terms.

2.3. Calculational details

Ab initio calculations at the Hartree-Fock HF/6-31G* and the density functional theory with Becke3LYP correlation (B3LYP/6-31G*) were carried out for the cations using the Gaussian 98 package [10]. The excited states were calculated with single configuration interaction (CIS) of 25 occupied and 25 unoccupied orbitals. A full optimisation of the ground and excited state potential minima was performed and controlled by vibrational analysis (Hessian matrix).

Comparative semiempirical ground state calculations were also carried out using AM1 [11] and PM3 [12]

* Corresponding author. Fax: +49-30-2093-5553.
E-mail address: vlad@chemie.hu-berlin.de (V.A. Kharlanov).

1010-6030/01/$ – see front matter
PII: S1010-6030(01)00436-1

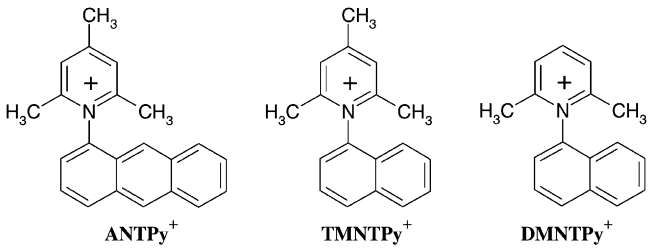

Scheme 1. The investigated pyridinium cations.

Hamiltonians with the aid of the AMPAC 5.0 package [13]. The calculations of transition energies and oscillator strengths were done using the CNDO/S–CI method with interaction of 100 singly excited configurations and the parameters sets described in [14] for the fully optimised AM1 ground state structures. The ZINDO/S calculation with single configuration interaction of 10 occupied and 10 unoccupied orbitals was carried out using the Gaussian 98 package [10].

3. Results and discussion

3.1. Absorption spectra of *TMNTPy*$^+$

The absorption spectrum of **TMNTPy**$^+$ has three low energy bands (Fig. 1a and Table 1). The distinct long wavelength absorption band at 36,500 cm^{-1} is typical in position and intensity for various methyl substituted pyridinium cations [15] and has a weakly pronounced vibrational structure. A comparison with the vibrational structure of naphthalene (Fig. 1b) shows that the absorption band of the latter is considerably more structured. Similar to *N*-phenyl-2,4,6-trimethylpyridinium [16] and ANTPy$^+$ [2], the most stable geometry of **TMNTPy**$^+$ in the ground state is a twisted one with the fragments in perpendicular planes because of sterical hindering due to the methyl groups in the 2,6 position of the heterocyclic ring. Therefore, the absorption band at 36,500 cm^{-1} is a superposition of the absorption bands of the fragment transitions with locally excited nature. The positions of the other absorption bands

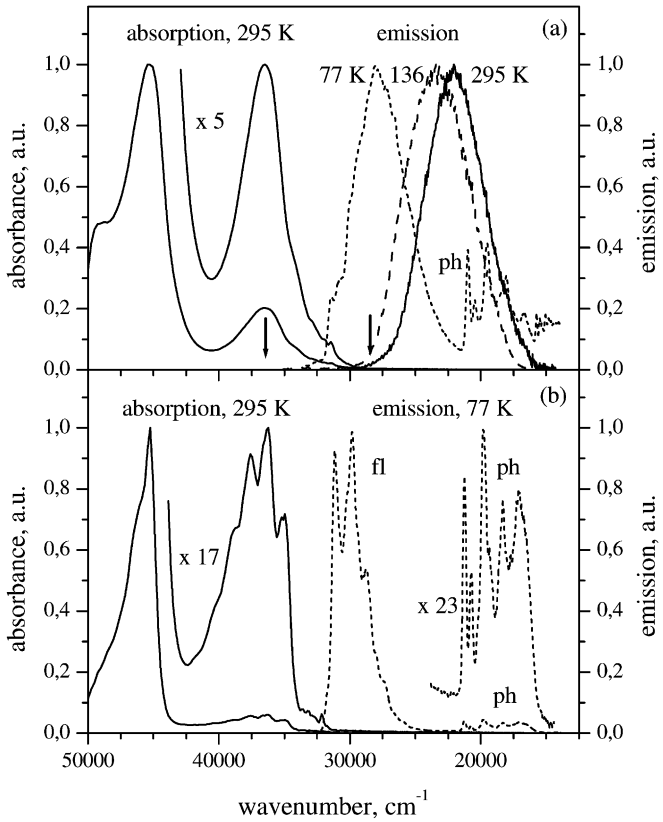

Fig. 1. The absorption and corrected emission spectra of **TMNTPy**$^+$ (a) and naphthalene (b) in ethanol at 295, 136 and 77 K. The arrows indicate two excitation energies which result in identical emission spectra.

at 45,450 and 49,100 cm^{-1} (shoulder) coincide with the naphthalene bands (Fig. 1a and b) and have also a mixed nature. A weak intensity absorption band with charge shift CSh nature analogously as for **ANTPy**$^+$ [1–3] lacks in the spectrum of **TMNTPy**$^+$ and is probably hidden below the more intensive absorption bands.

3.2. Ground state geometry

Semiempirical (AM1 and PM3) and ab initio (HF/6-31G* and B3LYP/6-31G*) calculations (Table 2) show that the

Table 1
Experimental absorption bands of **TMNTPy**$^+$ (EtOH, 295 K) and calculated transitions (CNDO/S, ZINDO/S and HF/6-31G* with CIS)

ΔE_a (eV)–ν_f (cm^{-1}) (experimental)	Absorption transition[a] CNDO/S	Absorption transition[a] ZINDO/S	Absorption transition[b] HF/6-31G*-CIS
3.90–31450 sh	3.53 (0.0001) CSh 4.07 (0.0060) LE^{1}L$_b$ Naph	3.28 (0.0009) CSh 3.92 (0.0060) LE^{1}L$_b$ Naph	5.58 (0.0145) LE^{1}L$_b$ Naph 5.73 (0.1321) LE^{1}L$_a$ Naph
4.52–36500	4.41 (0.1453) LE^{1}L$_a$ Naph 4.44 (0.1062) LE Py+	4.32 (0.1275) LE^{1}L$_a$ Naph 4.35 (0.0820) LE Py+	5.85 (0.0003) CSh 6.25 (0.2877) LE Py+
5.63–45450	5.47 (0.3040) LE Naph 5.57 (0.2490)	5.87 (0.8020) LE Naph	–
6.02–49020 sh	5.62 (0.1074) LE Naph	5.95 (0.2668) LE Naph	–

[a] For the AM1 optimized ground state geometry of **TMNTPy**$^+$.
[b] For the HF/6-31G* optimized ground state geometry of **TMNTPy**$^+$.

Table 2
Some geometry characteristics of the S_0 state optimized equilibrium geometry of **TMNTPy**$^+$ by AM1, PM3, HF/6-31G* and B3LYP/6-31G*

Bond distance (Å) and torsion angle (°)	AM1	PM3	HF/6-31G*	B3LYP
N1–2	1.3814	1.3871	1.3583	1.3742
2–3	1.4023	1.3940	1.3733	1.3868
3–4	1.4023	1.3986	1.3910	1.4001
N1–7	1.4442	1.4635	1.4583	1.4643
7–8	1.3894	1.3815	1.3567	1.3770
8–9	1.4100	1.4076	1.4129	1.4133
9–10	1.3739	1.3717	1.3581	1.3764
10–11	1.4204	1.4193	1.4200	1.4205
11–12	1.4232	1.4228	1.4196	1.4206
12–13	1.3728	1.3682	1.3579	1.3760
13–14	1.4152	1.4143	1.4147	1.4152
14–15	1.3746	1.3696	1.3597	1.3780
15–16	1.4214	1.4213	1.4207	1.4211
16–7	1.4366	1.4293	1.4232	1.4248
4–N1–7	179.59	179.42	179.98	179.87
2–1–7–8 (α^a)	86.57	89.83	89.90	89.85
β^a	0.41	0.58	0.02	0.13

[a] For definitions of α and β see Figs. 2 and 3.

TMNTPy$^+$ cation in the S_0 state possesses a perpendicular geometry (Fig. 2). The geometrical parameters determined are very similar for the different methods (Table 2). The cation fragments are perpendicular to each other and the bond distances are alternating in a similar way for the various methods.

3.3. Nature of the absorption band

Semiempirical calculations (CNDO/S, ZINDO/S and HF/6-31G*-CIS) were carried out for the fully optimised ground state geometry and show that in fact the long wavelength absorption band is composed by the superposition of transitions having locally excited nature. The transitions LE^1L_a and LE^1L_b (Table 1) are localised on the naphthalene fragment and have polarisation's along the long and short axes of the fragment, respectively, as in unsubstituted naphthalene. The transition LE is localised on the pyridinium fragment and lies in the same energy range. The CSh transition is of forbidden nature with charge shift from the electron donor (naphthalene fragment) to the electron acceptor (heterocyclic ring). The results obtained are analogous to the results for **ANTPy**$^+$ [2]. The transition energies obtained with the ab initio method are considerably higher than the experimental values and are estimated less reliable. High quality ab initio calculations (CASSCF and CASMP2) have been performed for small molecules [17] but are not appropriate for the size of molecules studied here. The semiempirical calculation results indicate that the lowest energy transition has CT nature. In view of the ionic character of the molecule studied, the transition is, therefore, termed charge shift (CSh). The weak absorption feature at 30,500 cm^{-1} (to the red of the naphthalene 0–0 transition) may correspond to this forbidden CSh absorption. The short wavelength bands of **TMNTPy**$^+$ are mainly formed by the local naphthalene transitions.

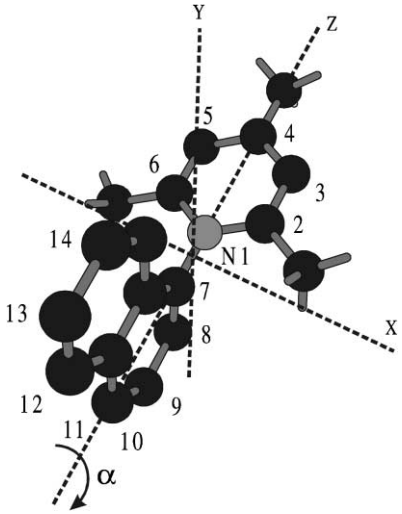

Fig. 2. The fully optimized S_0 geometry of **TMNTPy**$^+$ and the atom numeration.

3.4. Fluorescence

The **TMNTPy**$^+$ cation exhibits a weak ($\Phi_f = 0.07$) structureless emission band ($\nu_f = 22{,}070\,cm^{-1}$) with large Stokes shift ($\Delta\nu_{a-f} = 14{,}430\,cm^{-1}$) (ethanol, 296 K, Table 3 and Fig. 1a) no matter where the excitation occurs. This large Stokes shift is indicative of large geometry changes in the S_1 state, or of a strong change of the electronic character.

Cooling of the solution shifts the fluorescence band moderately to the blue ($\nu_f = 23{,}750\,cm^{-1}$, $\nu_{a-f} = 14{,}430\,cm^{-1}$, EtOH, 136 K) and increases the fluorescence intensity ($\Phi_f = 0.18$, EtOH, 150 K) (Table 3 and Fig. 1a).

At 77 K, the emission of **TMNTPy**$^+$ is shifted to the shorter wavelength range ($\nu_f = 28{,}010\,cm^{-1}$) but the

Table 3
Maximum of the fluorescence band[a] (ν_f and ΔE_f), Stokes shift[b] ($\Delta\nu_{a-f}$), fluorescence quantum yield (Φ_f) and decay time (τ_f) of **TMNTPy**$^+$ at various temperatures in EtOH

Fluorescence parameter	77 K	136 K	296 K
ν_f (cm^{-1}) (ΔE_f (eV))	28010 (3.47)	23750 (2.94)	22070 (2.74)
$\Delta\nu_{a-f}$ (cm^{-1})	8490	12750	14430
Φ_f	0.7 ± 0.2[c]	0.18[d]	0.07
τ_f (ns)	3.0	2.6[e]	2.3
τ_r (ns)	4.3 ± 0.8	14.8	34.3

[a] Disregarding the vibrational structure for 77 K.
[b] Difference between absorption and fluorescence maximum.
[c] From an extrapolation of the temperature dependence of the fluorescence quantum yield.
[d] At 150 K.
[e] Average decay time of biexponential fit (Table 4).

Table 4
Wavelength dependence of the fluorescence decay parameters of **TMNTPy**$^+$ at various temperatures in EtOH

Temperature (K)	Decay Parameter	25000 cm^{-1}	23800 cm^{-1}	22700 cm^{-1}
303	τ (ns)	2.3 ± 0.1	2.3 ± 0.1	2.4 ± 0.1
143	τ_1 (ns) (A_1)	1.39 (0.59)	2.03 (0.63)	2.39 (0.57)
	τ_2 (ns) (A_2)	3.12 (0.41)	3.62 (0.37)	3.50 (0.43)
	$\langle\tau\rangle$ (ns)	2.09	2.62	2.87
77	τ (ns)	3.0 ± 0.2	–	3.1 ± 0.2

Stokes shift with respect to the absorption maximum is still large ($\nu_{a-f} = 8490\,cm^{-1}$). The emission exhibits a weakly pronounced vibrational structure resembling the napthalene emission in the blue wing (Fig. 1). However, the main part of the spectrum is considerably red-shifted as compared to naphthalene. This broad fluorescence band at 77 K can be interpreted by the simultaneous emission from two species one of which corresponds to the naphthalene emission of locally excited nature (structured component, Fig. 1a and b) and the other one to a more redshifted unstructured component. In contrast to **TMNTPy**$^+$, **ANTPy**$^+$ at 77 K has only the anthracene-like emission [1,3].

3.5. Phosphorescence

At 77 K, **TMNTPy**$^+$ exhibit a phosphorescence band with a position and vibrational structure characteristic for the phosphorescence of unsubstituted naphthalene (Fig. 1a and b). The T_1 state of **TMNTPy**$^+$ is, therefore, localised on the naphthalene fragment.

3.6. Fluorescence decay

The fluorescence decay at room temperature is single exponential, corresponding to a moderately forbidden emission ($\tau_r = 34$ ns, Table 3). At lower temperature, the fluorescence kinetics show multiexponential character, depending on the emission wavelength (Table 4). Part of this relaxation may be due to relaxation from the LE to the CS state, and a further part of the relaxation can be attributed to the time-dependent Stokes-shift of the CS-band, as observed for other compounds with significant charge shift [18].

3.7. Excited state structures

In a search of the possible relaxed structures of the LE and CSh excited states of the investigated *N*-naphtyl-pyridinium, the compound **DMNTPy**$^+$ lacking the methyl group in 4-position of the pyridinium ring is used as a model cation of **TMNTPy**$^+$ (Scheme 1).

The ab initio calculation (HF/6-31G*-CIS) which used the fully optimised S_0 equilibrium geometry as a start geometry resulted in a stable structure of LE character and with Cs symmetry (Fig. 3). The geometrical parameters (Table 5) of this structure are characterised by only insignificant changes of bond distances as compared to the S_0 state geometry (Table 2). The transition is partially forbidden ($f = 0.0196$) and is localised on the naphthalene fragment with a polarisation along the long axis of the fragment (Table 6). The positive charge is localised on the pyridinium fragment.

In search of a twisted structure with a charge shift or biradicaloid nature the fully optimized S_1 geometry of the *N*-phenylpyridinium cation [19] with a similar CS nature is used as start geometry. The most significant feature of this structure is a bent geometry of the pyridinium ring due to pyramidalisation of the nitrogen atom. The bent ring can have two possible arrangements with respect to the naphthalene fragment. The two calculated stable structures with Cs symmetry 90A and 90B are shown in Fig. 3. They both have a bent and 90° twisted geometry with increased bond distances of N1–2 and N1–6 for the pyridinium ring and of 7–8 and 16–7 for the naphthalene moiety in relation to the distances of the LE structure (Table 5). The structures 90A and 90B are characterised by full charge shift from the pyridinium to the naphthalene fragment (Table 6). The transition to the ground state is polarised direct normally to a line connecting the fragments (*x*-axis, Fig. 2). The different bending orientations of the pyridinium fragment in structures 90A and 90B cause a slight difference of the state energy and oscillator strength. The energy gap between the S_1 and the triplet state with a similar electronic configuration is small (Table 6) indicating that each of these states possesses a nearly isoenergetic triplet state, a characteristic of biradicaloid charge transfer states [20].

The estimation of the radiative lifetime of the cation at 77 K (4.54 ns, Table 3) indicates that a relaxed S_1 structure with an allowed transition is also possible which leads to the redshifted emission maximum (Fig. 1a). This property can be realised in a geometry which permits the interaction of the cation fragments. In search of such a structure, a torsional angle 70° between the fragments and the bond distances of 90A were used as a start geometry for optimisation in the S_1 excited state. The calculations result in a stable structure with strong charge transfer character (structure CSh in Fig. 3) with a torsional angle 67.31° and bond distances very similar to the LE structure (Table 5). This structure is characterised by resonance between the two moieties and an allowed transition ($f = 0.2085$) with a transition energy 4.58 eV (Table 6). In contrast to the biradicaloid CSh state the resonance CSh state has a large $S_1 - T_1$ energy

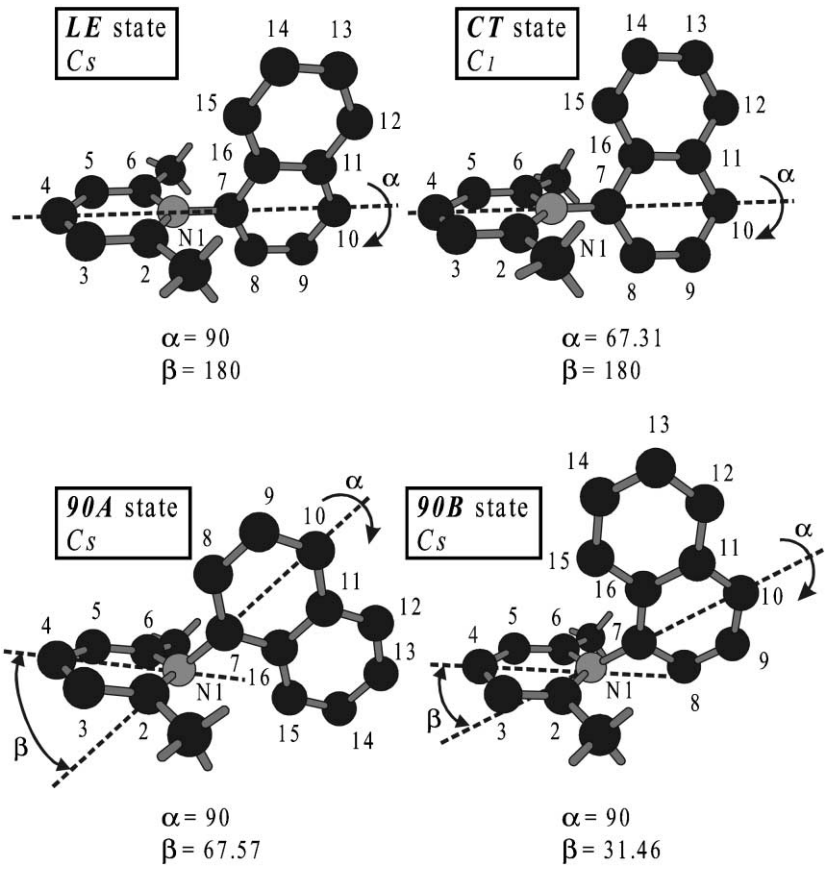

Fig. 3. The fully optimized S_1 equilibrium structures of **DMNTPy**$^+$: LE (Cs symmetry), CSh (Cs symmetry), 90A (Cs symmetry) and 90B (Cs symmetry) by HF/6-31G*-CIS. The structures differ mainly by the value of twist (a) and bending (b) of the pyridinium group as well as by the transition moment to the ground state and the amount of charge transfer to the pyridinium ring (see text).

Table 5
Some geometry characteristics of the T_1 and S_1 states optimized equilibrium structures of **DMNTPy**$^+$ by HF/6-31G* with interaction of singly excited configurations

Bond distance (Å) and twist or torsion angle (°)	T_1	S_1			
	LE	LE	CSh	90A	90B
N1–2	1.3573	1.3578	1.3907	1.4287	1.4244
2–3	1.3767	1.3769	1.3603	1.3598	1.3562
3–4	1.3832	1.3831	1.3960	1.4009	1.4026
N1–7	1.4563	1.4567	1.3907	1.4068	1.4002
7–8	1.4300	1.3894	1.4167	1.4177	1.4120
8–9	1.3544	1.4097	1.3741	1.3802	1.3763
9–10	1.4283	1.3898	1.3986	1.3862	1.3942
10–11	1.4035	1.4045	1.4028	1.4181	1.4057
11–12	1.4043	1.4042	1.4052	1.3948	1.4021
12–13	1.4353	1.3893	1.3914	1.3931	1.3926
13–14	1.3545	1.4060	1.3800	1.3825	1.3795
14–15	1.4285	1.3948	1.4033	1.3946	1.4036
15–16	1.4098	1.4015	1.3942	1.3980	1.3998
16–7	1.4011	1.4062	1.4289	1.4191	1.4208
4–N1–7	178.92	179.28	179.81	132.43	−148.54
2–1–7–8	89.20	89.56	67.31	69.05	103.21
α[a]	90.00	90.00	67.31	90.00	90.00
β[a]	1.08	0.72	0.19	47.57	−31.46

[a] For definitions of α and β see Fig. 3.

Table 6
Characteristics of T_1 and S_1 states for different optimized equilibrium structures of **DMNTPy**$^+$ by HF/6-31G*-CIS

Characteristic	T_1	S_1			
	LE	LE	CSh	90A	90B
Sum of electronic and zero-point energy (a.u.)	−706.958746	−706.860555	−706.866470	−706.867162	−706.867572
Lowest vibrational frequency (cm^{-1})	52.7	45.4	30.0	31.1	30.8
Transition energy of $S_1 \rightarrow S_0$ (eV)	2.185	5.147	4.583	3.807	4.180
Oscillator strength	0.0000	0.0196	0.2085	0.0066	0.0001
S_1–T_n energy gap (eV)	–	0.906[a]	1.977[b]	−0.175[a]	0.024[c]
Charge of pyridinium fragment in S_1 (S_0)	0.54 (0.53)	0.53 (0.54)	−0.02 (0.53)	−0.08 (0.61)	−0.15 (0.58)
Assignment	LE (Naph)	LE (Naph)	Resonance CSh	Biradicaloid CSh	Biradicaloid CSh

[a] T_3 state having equal electron configuration.
[b] T_1 state having equal electron configuration.
[c] T_4 state having equal electron configuration.

gap (1.98 eV) and the amount of charge transfer is comparable to that of the biradicaloid CS 90A and 90B minima (Table 6).

For the study of the T_1 state, all the S_1 state stable structures were used as the start geometries. But after optimisation, all these structures relaxed to a common 90° twisted stable minimum (lowest vibrational frequency is 52.7 cm^{-1}) geometry with Cs symmetry (Table 5) and small charge shift. (Table 6). In contrast to the S_1 locally excited state, the T_1 state geometry shows strong bond alternation in the naphthalene fragment because the bond distances 7–8, 9–10, 12–13, and 14–15 are increased and the bond lengths 8–9, and 13–14 are decreased (Table 5) but the nature of the state is also LE. This result explains the very good agreement between the phosphorescence spectra of naphthalene and the **TMNTPy**$^+$ cation (Fig. 1a and b).

4. Conclusion

The *N*-naphthyl-pyridinium cation shows multiple emission as a result of the formation of various equilibrium structures in the S_1 state. Three categories could be characterised by combining lifetime experiments and quantum chemical calculations: an S_1 (LE) state with locally excited character and weak charge shift, and two types of states with strong naphthalene-to-pyridinium charge shift character: (a) a resonance-type CS state with allowed transition moment and partial twisting (ca. 70°) and (b) two minima of a biradicaloid CS shift state with orthogonal fragments (90° twist) but bent geometry of the pyrimidinium ring and characterised by a forbidden transition moment and a very close lying triplet state.

Acknowledgements

The financial support by the Volkswagen Stiftung is gratefully acknowledged. We gratefully acknowledge the generous help of N. Makarova who provided the compound to us.

References

[1] V.A. Kharlanov, M.I. Knyazhansky, N.I. Makarova, V.A. Lokshin, J. Photochem. Photobiol. A: Chem. 70 (1993) 223.
[2] V.A. Kharlanov, M.I. Knyazhansky, W. Rettig, J. Mol. Struct. 380 (1996) 113.
[3] V.A. Kharlanov, W. Rettig, M.I. Knyazhansky, N. Makarova, J. Photochem. Photobiol. A: Chem. 103 (1997) 45.
[4] A.T. Balaban, A. Dinculescu, G.N. Dorofeenko, G.W. Fischer, A.V. Koblik, V.V. Mezheritskii, W. Schrith, in: A.R. Katritzky (Ed.), Pyrilium Salts: Synthese, Reactions, and Physical Properties, Suppl. 2, Advances in Heterocyclic Chemistry, Academic Press, New York, 1982.
[5] I.B. Berlman, Handbook of Fluorescence Spectra of Aromatic Molecules, 2nd Edition, Academic Press, New York, 1971.
[6] J.B. Birks, Photophysics of Aromatic Molecules, Wiley/Interscience, New York, 1970.
[7] J.A. Riddick, W.B. Bunger, Organic Solvents, Wiley/Interscience, New York, 1980.
[8] R. Passerini, J.G. Ross, J. Sci. Instrum. 30 (1953) 214.
[9] M. Vogel, W. Rettig, Ber. Bunsenges. Phys. Chem. 91 (1987) 1241.
[10] M.J. Frisch, G.W. Trucks, H.B. Schlegel, G.E. Scuseria, M.A. Robb, J.R. Cheeseman, V.G. Zakrzewski, J.A. Montgomery Jr., R.E. Stratmann, J.C. Burant, S. Dapprich, J.M. Millam, A.D. Daniels, K.N. Kudin, M.C. Strain, O. Farkas, J. Tomasi, V. Barone, M. Cossi, R. Cammi, B. Mennucci, C. Pomelli, C. Adamo, S. Clifford, J. Ochterski, G.A. Petersson, P.Y. Ayala, Q. Cui, K. Morokuma, D.K. Malick, A.D. Rabuck, K. Raghavachari, J.B. Foresman, J. Cioslowski, J.V. Ortiz, A.G. Baboul, B.B. Stefanov, G. Liu, A. Liashenko, P. Piskorz, I. Komaromi, R. Gomperts, R.L. Martin, D.J. Fox, T. Keith, M.A. Al-Laham, C.Y. Peng, A. Nanayakkara, C. Gonzalez, M. Challacombe, P.M.W. Gill, B. Johnson, W. Chen, M.W. Wong, J.L. Andres, C. Gonzalez, M. Head-Gordon, E.S. Replogle, J.A. Pople, Gaussian 98, Revision A.7, Gaussian, Pittsburgh, PA, 1998.
[11] M.J.S. Dewar, E.G. Zoebisch, E.F. Healy, J.J.P. Stewart, J. Am. Chem. Soc. 107 (1985) 3202.
[12] J.J.P. Stewart, J. Comp. Chem. 10 (1989) 209.
[13] M.J.S. Dewar, J.J.P. Stewart, J.M. Ruiz, D. Liotard, E.F. Healy, R.D. Dennington II, AMPAC 5.0, Semichem, Shawnee, 1994.
[14] H.M. Chang, H.H. Jaffe, C.A. Masmanidis, J. Chem. Phys. 79 (1109) (1975) 1118.
[15] M.E. Kosover, S.W. Bauer, J. Am. Chem. Soc. 82 (1960) 2191.
[16] A.T. Balaban, M.D. Gheorghin, Rev. Roum. Chim. 23 (1978) 1065.
[17] W. Sudholt, A.L. Sobolewski, W. Domcke, Chem. Phys. 240 (1999) 9.
[18] M.J. Van der Meer, H. Zhang, W. Rettig, M. Glasbeek, Chem. Phys. Lett. 320 (2000) 673.
[19] V. Kharlanov, W. Rettig, unpublished result.
[20] J. Michl, V. Bonacic-Koutecký, Electronic Aspects of Organic Photochemistry, Wiley, New York, 1990.